Orientation induces adsorption of the hydrated proton at the air-water interface

Shavkat I. Mamatkulov,[1,2] Christoph Allolio,[1,3]

Roland R. Netz,[1] and Douwe Jan Bonthuis[1,*]

[1]*Fachbereich Physik, Freie Universität Berlin, 14195 Berlin, Germany*

[2]*Center of Higher Technologies, 100174 Tashkent, Uzbekistan*

[3]*The Fritz Haber Research Center, The Hebrew*

University of Jerusalem, Jerusalem 91904, Israel

(Dated: September 11, 2017)

Abstract

The surface tension of the air-water interface increases upon the addition of inorganic salts, implying a negative surface excess of ionic species. Acids, however, induce a lower increase or, depending on anion type, even a *decrease* in surface tension, indicating a positive surface excess of hydrated protons. In combination with the apparent negative charge at pure air-water interfaces derived from electrokinetic experiments, this experimental fact has presented a source of intense debate since the second half of the 19th century. Here, we calculate surface tensions and ionic surface propensities at air-water interfaces from classical thermodynamically consistent molecular dynamics simulations. The surface tensions of NaOH, HCl and NaCl solutions show outstanding quantitative agreement with experiment at all concentrations. Of the studied ions, only H_3O^+ adsorbs to the air-water interface. The adsorption can be explained by the deep attractive potential well caused by the orientation of the H_3O^+ dipole in the interfacial electric field, which reflects enhanced proton hydrogen bonding capability at the interface. *Ab initio* simulations confirm the interfacial orientation of H_3O^+ and H_2O.

Introduction. – It is hard to imagine a more long-standing and fundamental controversy in physical chemistry than the one concerning the affinity of protons for air-water interfaces and hydrophobic surfaces [1]. Ions at interfaces are subject to a range of forces, including steric and van der Waals interactions, as well as electrostatic forces caused by surface potentials and the inhomogeneity of the dielectric environment. The resulting interfacial adsorption or depletion of ions dominates the interaction between air bubbles [2, 3] and uncharged lipid membranes [4], as well as nanoparticle assembly [5] and the stability of colloidal suspensions [6]. The air-water interface, being the simplest aqueous interface, is the pivotal case for understanding the intricate properties of aqueous solutes. Onsager & Samaras showed that the image charge repulsion is expected to induce a depletion of ions from the interfacial layer, leading to an increase in surface tension with increasing salt concentration [7]. For most types of salt, this is confirmed experimentally, with the extent of the surface tension increment depending mainly on the valency of the ion [3, 8–10]. However, the surface tension of many acids *decreases* [3, 8–10]. Via the Gibbs isotherm, a decrease in surface tension rigorously implies a positive surface excess of ions, without any approximation involved. Because the decrease is consistently found for acids only, the rational conclusion is that protons adsorb at the air-water interface [9, 11]. Sum-frequency and second-harmonic generation experiments confirm the enhanced concentration of H_3O^+ at the air-water interface [12–15].

The situation is confounded, however, by the results from kinetic and force measurements. Electrophoresis measurements [16–19] and measurements of the disjoining pressure of thin films [20–22] consistently indicate that the clean air-water interface at neutral pH is negatively charged. Also measurements on oil-water emulsions at pH=9 show a decreasing pH with increasing total surface area, suggesting OH^- adsorption [23]. Although the experiments are unambiguous, the ionic surface propensies are inferred through theoretical models, involving assumptions for the kinetic properties of the interface, such as the viscosity, the dielectric response, possible charge transfer [24] and confinement-induced enhancement of the water auto-dissociation constant [25]. Calculations using the extended Poisson-Boltzmann [26] or hypernetted chain approximations [27] show that dispersion, image charge and solvation interactions are important to qualitatively reproduce ion-specific adsorption, but quantitative agreement with surface tension experiments remains elusive. For H_3O^+ and OH^-, classical molecular dynamics (MD) simulations have been performed using heuristic force fields, giving mixed results [28, 29]. Likewise, *ab initio* molecular dy-

namics (OH$^-$ adsorption [30, 31], H$_3$O$^+$ adsorption [28]) lead to disparate conclusions. Other computational methods, such as emperical valence-bond based reactive molecular dynamics [32–34] and continuum methods [35], show H$_3$O$^+$ adsorption and therefore qualitative agreement with surface tension measurements. Quantitative agreement is still inadequate, however, owing to the sensitivity of the surface excess to the adsorption potential [35, 36]. An explicit calculation of the surface tension of acids using MD simulations has not been attempted so far.

In this paper, we report on the calculation of both the surface tension and the individual surface propensities of H$_3$O$^+$ and OH$^-$ using MD simulations. Importantly, we use a thermodynamically consistent approach, requiring that the water-water, ion-water and ion-ion interactions are reproduced accurately and in agreement with the known macroscopic thermodynamic properties. This is accomplished by using force fields for the ions (H$_3$O$^+$, OH$^-$, Na$^+$, Cl$^-$) which have been optimized to reproduce the macroscopic experimental solvation free energy (determined by the ion-water interactions) and the activity of the ion pairs as a function of salt concentration (determined by the balance between ion-water and ion-ion interactions) [37]. For water, we use the SPC/E model [38], which reproduces the density, dielectric properties, structure factor and air-water surface tension with high accuracy. While the ions OH$^-$, Cl$^-$ and Na$^+$ are repelled from the air-water interface, we find that H$_3$O$^+$ is adsorbed with an energy of 1 $k_B T$, caused by its orientation with the hydrogen atoms pointing toward the water phase, which is favored by the interfacial electric field caused by the orientation of the water molecules. Note that the same behavior of adsorption and orientation has been previously proposed [39] and observed [12, 28, 32, 40], but a quantitative analysis has been lacking. Clearly, our classical simulation method will neither reproduce the proton dynamics, nor the intramolecular electronic structure, but this will not affect the macroscopic equilibrium thermodynamics we are investigating, because the effects of the intramolecular structure are accounted for by the force field optimization, which has been performed with respect to experimental properties. As a consistency check, we also perform *ab initio* simulations of the aqueous interface and show that the orientations of H$_2$O and H$_3$O$^+$ found in the classical simulations are in excellent agreement with the *ab initio* results.

Ion adsorption and the Gibbs isotherm. – We consider an interface of surface area A with surface tension γ, separating the water (w) and vapor (v) phases. Excess quantities pertaining to the surface are labeled σ. Adsorbed at the surface are N_i^σ particles of type i,

3

having chemical potential μ_i. The Gibbs isotherm relates the total ionic surface excess to the surface tension [41],

$$\mathrm{d}\gamma = -\sum_i \frac{N_i^\sigma}{A}\,\mathrm{d}\mu_i. \tag{1}$$

The number of adsorbed particles at a planar interface located at $z = z_0$ equals

$$\frac{N_i^\sigma}{A} = \int_{-\infty}^{z_0} \big(c_i(z) - c_i^v\big)\mathrm{d}z + \int_{z_0}^{\infty} \big(c_i(z) - c_i^w\big)\mathrm{d}z, \tag{2}$$

with c_i being the concentration of species i, and z being the coordinate perpendicular to the interface. Choosing z_0 equal to the Gibbs dividing surface z_{GDS} of the water (defined as the position for which the water excess vanishes), $N_{\mathrm{H_2O}}^\sigma = 0$ and the sum in Eq. 1 reduces to a sum over the ion species $+$ and $-$. Writing $\mathrm{d}\mu_i = k_B T \mathrm{d}\ln a_i$, with a_i being the ionic activity and k_B being Boltzmann's constant, we find

$$\mathrm{d}\gamma = -k_B T \sum_{i=\pm} \frac{\Gamma_i}{c_0} \frac{\mathrm{d}(\ln a_\pm)}{\mathrm{d}(\ln c_0)}\,\mathrm{d}c_0, \tag{3}$$

with c_0 being the bulk salt concentration, and $a_\pm = (a_+^p a_-^q)^{1/(p+q)}$ being the mean activity of a salt with stoichiometric coefficients p and q. The log-log-derivative $\mathrm{d}(\ln a_\pm)/\mathrm{d}(\ln c_0)$ is a function of c_0 which is close to 1 for moderate c_0. In Eq. 3, the ionic excess at the air-water interface is defined as

$$\Gamma_i = \int_{-\infty}^{z_{\mathrm{GDS}}} c_i(z)\mathrm{d}z + \int_{z_{\mathrm{GDS}}}^{\infty} \big(c_i(z) - c_0\big)\mathrm{d}z. \tag{4}$$

Therefore, the sign of $\mathrm{d}\gamma/\mathrm{d}c_0$ is determined by the sign of $\sum_i \Gamma_i$: $\mathrm{d}\gamma/\mathrm{d}c_0 < 0$ indicates adsorption, $\mathrm{d}\gamma/\mathrm{d}c_0 > 0$ indicates depletion. See Fig. 1 for simulation snapshots and density profiles $c_i(z)$, with z_{GDS} indicated. Information on the individual ionic surface propensities can be obtained from comparing ion pairs with one common species.

Experimental literature data. – The experimental data of the surface tension γ as a function of the salt concentration c_0 for ion pairs that fully dissociate in solution follow straight lines [3, 8]. We show the experimentally determined derivatives of these lines, $\mathrm{d}\gamma/\mathrm{d}c_0$, for different ion pairs in Fig. 2. The derivatives follow the anionic Hofmeister series, *i.e.* $\mathrm{d}\gamma/\mathrm{d}c_0$ decreases as ions become more chaotropic going from left to right [42]. For the salt solutions, the surface tension derivatives are all positive and similar for different cations, only depending on valency, as expected from Onsager & Samaras theory [7]. Strikingly, however, the surface tension derivatives for the acids are significantly lower for all ionic combinations,
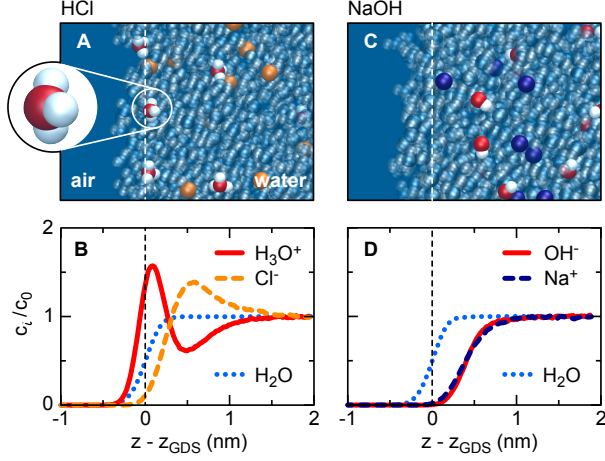
FIG. 1. Snapshots of the simulations (A and C) and density profiles $c_i(z)/c_0$ (B and D), where c_0 is the bulk salt concentration, as a function of $z - z_{\mathrm{GDS}}$, where z_{GDS} is the Gibbs dividing surface of the water. The solutions shown are HCl (A and B) and NaOH (C and D) at $c_0 \approx 0.5$ mol/l. The inset in (A) highlights the prevalent orientation of H_3O^+ with its hydrogen atoms pointing toward the water phase.
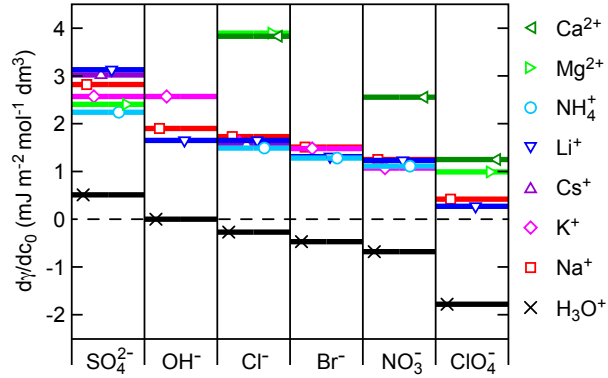

FIG. 2. Derivative of the experimental surface tension γ with respect to the salt concentration c_0 for different ion pairs. The data correspond to the averages of the literature data [3, 9].

and negative for all anions to the right of hydroxide. This provides clear evidence for the special effect of the solvated proton. Based on the experimental data, explanations other than a strong adsorption of protons to the interface are hard to rationalize.

Simulations at finite concentration. – We simulate a slab of water with different concentrations of NaOH, HCl and NaCl. Details are described in the Supplement [36]. Snapshots of the simulation box (cross section) are shown in Figs. 1 A and C. The corresponding den-
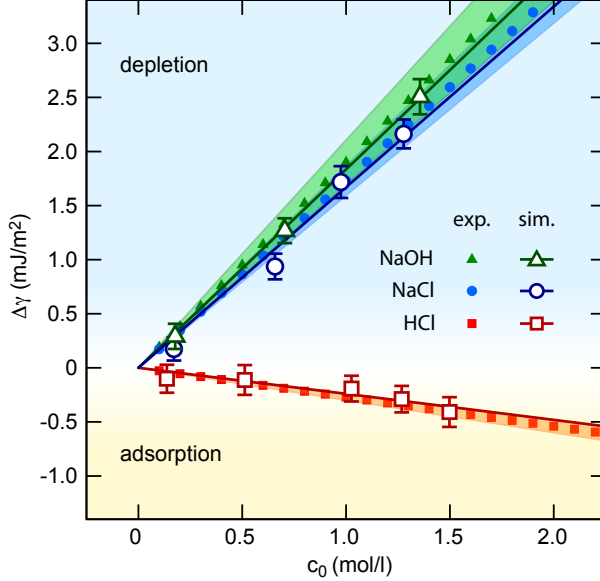
FIG. 3. Change of the air-water surface tension $\Delta\gamma$ as a function of the bulk salt concentration c_0, in experiments and classical simulations. The solid symbols correspond to the experimental data [3, 9], with the shaded area indicating the 90% confidence interval. The open symbols correspond to the simulations, where the surface tension has been calculated using Eq. 5. The solid lines are linear fits to the simulation data, used to calculate the surface excess shown in Fig. 5.

sity profiles are shown in Figs. 1 B and D. Whereas H_3O^+ is clearly present in the surface layer, OH^-, Cl^- and Na^+ primarily reside in the bulk.

We calculate the surface tension of the air-water interface from the anisotropy of the simulated stress tensor,

$$\gamma = \tfrac{1}{2} L_z \left(P_z - \tfrac{1}{2} \left(P_x + P_y \right) \right), \tag{5}$$

with L_z being the size of the simulation box in the direction perpendicular to the surface, the factor $\tfrac{1}{2}$ stemming from the fact that there are two interfaces in every simulation box, and P_z and $\tfrac{1}{2}(P_x + P_y)$ being the perpendicular and parallel components of the stress tensor, respectively. For all ion pairs tested, the surface tension increments $\Delta\gamma$, calculated as the difference between the simulated surface tension of the electrolytes and pure water, agree exceptionally well with the experimental data (Fig. 3). In particular, Fig. 3 demonstrates that the strongly enhanced concentration of H_3O^+ at the interface, shown in Fig. 1B, leads to $d\gamma/dc_0 < 0$ for HCl, which is not observed for any other ion pair, including NaCl.

Infinite dilution. – The simulations described in the previous section are performed at

6

relatively high salt concentration, $c_0 > 0.1$ mol/l. In fact, the salt concentration of the lowest HCl concentration corresponds to pH $= 0.8$. This is well beyond the isoelectric point ($2 < \text{pH} < 5$, depending on experimental conditions [17, 18]), meaning that at such high concentrations, also kinetic experiments indicate a positive surface charge. The experimental situation is more ambiguous at low concentration, where some electrolytes exhibit a shallow minimum in the surface tension ($c_0 \sim 10^{-3}$ mol/l), referred to as the Ray-Jones effect [43], and the kinetic measurements appear to indicate a negative surface charge [17, 18].

To study the surface propensity of H_3O^+ at neutral pH, we calculate the potential of mean force, V_{PMF}^i, of single ions ($i \in \{H_3O^+, OH^-, Cl^-, Na^+\}$) using umbrella sampling. Also for a single H_3O^+ ion, $V_{\text{PMF}}^{H_3O^+}$ exhibits a clear minimum around the position of z_{GDS}, with a depth of $\approx 1\ k_B T$ (Fig. 4A). The other ions are all expelled from the interfacial region, with $V_{\text{PMF}}^i \approx 3.5\ k_B T$ at $z = z_{\text{GDS}}$. At the clean air-water interface (pH $= 7$), the concentration $c_i \approx c_0 \exp\left[-V_{\text{PMF}}^i / k_B T\right]$ indeed indicates a surface excess of H_3O^+, with OH^- being expelled into the bulk (inset of Fig. 4A).

What causes the strong interfacial H_3O^+ adsorption? The left inset in Fig. 4B, showing the cosine of the angle θ between the dipole and the the z-axis from classical MD simulations, demonstrates that H_3O^+ is almost perfectly oriented with the hydrogen atoms facing the water phase (red solid line), a snapshot of which is shown in Fig. 1A. This orientation is consistent with vibrational sum-frequency experiments [14]. Also the interfacial water molecules tend to have a preferential orientation (blue solid line). The average orientations of the H_2O and H_3O^+ molecules from classical simulations are in excellent agreement with the results of *ab initio* simulations of the protonated oil-water surface (symbols in the left inset of Fig. 4B), see Supplementary Information for details [36]. At the air-water interface, a concordant H_2O orientation has been reported earlier using classical and *ab initio* simulations [44]. As the formation of hydrogen bonds in water depends on the relative orientation of the OH bonds, we use the dipole energy of the oriented H_3O^+ in the z-dependent interfacial electric field $E_z(z)$ caused by the oriented water molecules as a proxy for the hydrogen bonding capability. The sign of $E_z(z)$ (right inset of Fig. 4B) is in agreement with the results from *ab initio* simulations, taking into account that ions only probe the space between the water molecules [45]. Note that $E_z(z)$ includes contributions from electric moments of higher order than the dipole [46]. The z-dependent contribution to the free energy of the relative molecular orientations, $-|\mu|\langle \cos\theta \rangle E_z(z)$, with the H_3O^+ dipole moment being equal
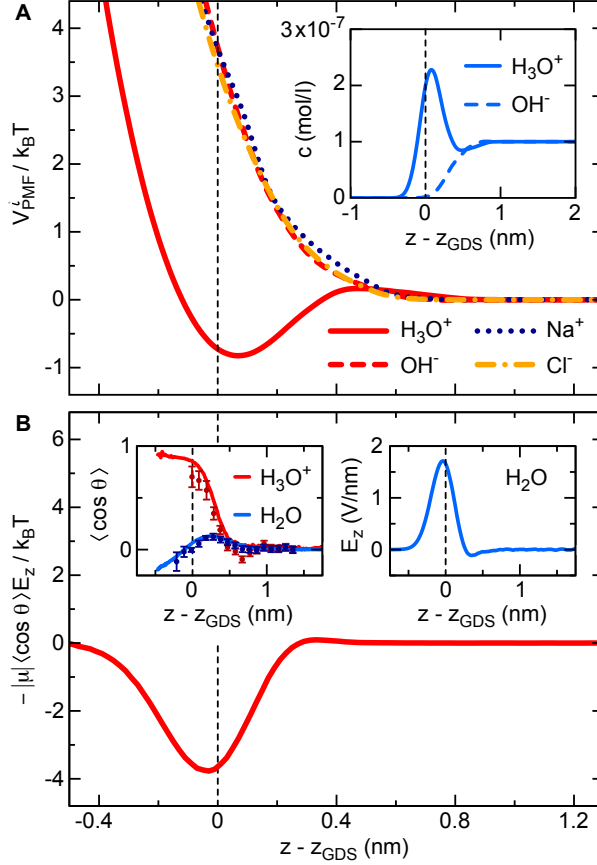
7

FIG. 4. (A) The potential of mean force, V_{PMF}^i, in units of $k_B T$, as a function of the distance to the Gibbs Dividing Surface, z_{GDS}, for four different ions. The inset shows the predicted ion density profiles, $c_i(z) \approx c_0 \exp\left[V_{\mathrm{PMF}}^i(z)\right]$, for pure water at pH $= 7$ ($c_0 = 10^{-7}$ mol/l). (B) The dipole contribution to the energy of an H_3O^+ ion, $-|\mu|E_z\langle\cos\theta\rangle$. The orientation of H_3O^+ and H_2O are shown in the left inset, calculated from classical simulations at $c_0 = 1$ mol/l (solid lines) and *ab initio* simulations at $c_0 = 5$ mol/l (symbols). The *ab initio* simulations have been performed at the hexane-water interface in order to better localize the surface [36]. The z-dependent classical electric field $E_z(z)$ at the pure air-water interface, caused by the water orientation, is shown in the right inset.

to $|\mu| = 0.066\, e\,$nm [37], exhibits an attractive well of $\approx 4\, k_B T$ (Fig. 4B). Using an extended point charge distribution instead of an ideal dipole gives a similar result [36]. Although other contributions, such as van der Waals and image charge interactions, are expected to play a role as well, the deep attractive well shown in Fig. 4B demonstrates that the dipole orientation energy is sufficient to explain the interfacial proton adsorption. This favorable
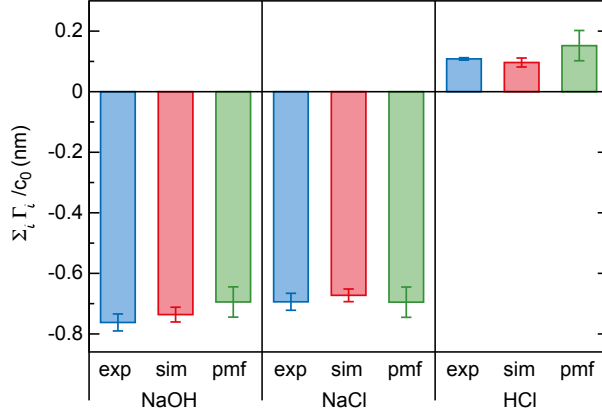
FIG. 5. Rescaled ionic excess $\sum_{i=\pm} \Gamma_i/c_0$ at the air-water interface for NaOH, NaCl and HCl. Columns correspond to experimental values (denoted *exp*), simulations at finite c_0 using $\sum_{i=\pm} \Gamma_i/c_0 = -(d\gamma/dc_0)/(k_B T)$ (from the linear fit to γ versus c_0 shown in Fig. 3, denoted *sim*), and calculations at vanishing c_0 using the simulated potentials of mean force (Eq. 6, denoted *pmf*).

relative orientation of the H_3O^+ and water dipoles identifies enhanced hydrogen bonding capability at the interface as the mechanism for the proton's interface activity.

Surface excess. – The rescaled surface excess for NaOH, NaCl and HCl at finite ion concentration is calculated from a linear fit to the simulations (solid lines in Fig. 3), using $\sum_{\pm} \Gamma_{\pm}/c_0 = -(d\gamma/dc_0)/(k_B T)$. The calculated surface excess values, denoted *sim*, are in excellent agreement with experimental results, denoted *exp* (Fig. 5). At vanishing ion concentration, we calculate the surface excess from $V_{PMF}^i(z)$,

$$\frac{\Gamma_i}{c_0} = \int_{-\infty}^{z_{GDS}} e^{-V_{PMF}^i} \, dz + \int_{z_{GDS}}^{\infty} \left(e^{-V_{PMF}^i} - 1 \right) \, dz. \tag{6}$$

Also at vanishing ion concentration, denoted *pmf*, the calculated surface excess values agree remarkably well with experiments and simulations at finite c_0 (Fig. 5), demonstrating the consistency of our approach.

Discussion and conclusions. – Classical simulations of the air-water interface using a thermodynamically consistent approach indicate that H_3O^+ is adsorbed at the air-water interface at all concentrations, in quantitative agreement with surface tension measurements. The adsorption can be understood in terms of the orientation of H_3O^+ in the interfacial water layer. The orientations found in *ab initio* simulations corroborate this adsorption mechanism. At low pH, the emerging picture of adsorbed protons at the interface is also in line with kinetic measurements of the ζ-potential. At neutral pH, however, the adsorption

9

of protons found in this study is in apparent contradiction with a naive interpretation of the kinetic measurements. This is not a fundamental contradiction, however, since it should be kept in mind that apart from surface propensity, kinetic measurements probe various other interfacial properties, such as the surface viscosity and the dielectric response. In fact, the strong preferential orientation affecting the surface propensity will also influence the kinetics of H_3O^+, as has been shown previously [47]. We conclude that experiments and thermodynamically consistent molecular dynamics simulations quantitatively agree: H_3O^+ adsorbs at the air-water interface.

ACKNOWLEDGEMENTS

* d.j.bonthuis@fu-berlin.de

[1] R. J. Saykally, Nat. Chem. **5**, 82 (2013).

[2] V. S. J. Craig, B. W. Ninham, and R. M. Pashley, Nature **364**, 317 (1993).

[3] C. L. Henry, C. N. Dalton, L. Scruton, and V. S. J. Craig, J. Phys. Chem. C **111**, 1015 (2007).

[4] H. I. Petrache, T. Zemb, L. Belloni, and V. A. Parsegian, Proc. Nat. Acad. Sci. USA **103**, 7982 (2006).

[5] Y. Min, M. Akbulut, K. Kristiansen, Y. Golan, and J. Israelachvili, Nat. Mater. **7**, 527 (2008).

[6] C. Calero and J. Faraudo, J. Am. Chem. Soc. **133**, 15025 (2011).

[7] L. Onsager and N. N. T. Samaras, J. Chem. Phys. **2**, 528 (1934).

[8] P. K. Weissenborn and R. J. Pugh, J. Colloid Interface Sci. **184**, 550 (1996).

[9] L. M. Pegram and M. T. Record, Jr., J. Phys. Chem. B **111**, 5411 (2007).

[10] Y. Marcus, J. Chem. Eng. Data **55**, 3641 (2010).

[11] L. M. Pegram and M. T. Record, Jr., Proc. Nat. Acad. Sci. USA **103**, 14278 (2006).

[12] P. B. Petersen and R. J. Saykally, J. Phys. Chem. B **109**, 7976 (2005).

[13] L. M. Levering, M. R. Sierra-Hernández, and H. C. Allen, J. Phys. Chem. C **111**, 8814 (2007).

[14] C. Tian, N. Ji, G. A. Waychunas, and Y. Ron Shen, J. Am. Chem. Soc. **130**, 13033 (2008).

[15] S. Yamaguchi, A. Kundu, P. Sen, and T. Tahara, J. Chem. Phys. **137**, 151101 (2012).

[16] G. Quincke, Ann. Phys. Chem. **113**, 513 (1861).

[17] C. Yang, T. Dabros, D. Li, J. Czarnecki, and J. H. Masliyah, J. Colloid Interface Sci. **243**, 128 (2001).

[18] M. Takahashi, J. Phys. Chem. B **109**, 21858 (2005).

[19] P. Creux, J. Lachaise, A. Graciaa, and J. K. Beattie, J. Phys. Chem. C **111**, 3753 (2007).

[20] D. Exerowa, Kolloid Z. Z. Polym. **232**, 703 (1969).

[21] K. Karraker and C. Radke, Adv. Colloid Interface Sci. **96**, 231 (2002).

[22] N. Schelero and R. von Klitzing, Soft Matter **7**, 2936 (2011).

[23] J. K. Beattie and A. M. Djerdjev, Angew. Chem. Int. Ed. **43**, 3568 (2004).

[24] R. Vácha, O. Marsalek, A. P. Willard, D. J. Bonthuis, R. R. Netz, and P. Jungwirth, J. Phys. Chem. Lett. **3**, 107 (2012).

[25] D. Muñoz-Santiburcio and D. Marx, Phys. Rev. Lett. **119**, 056002 (2017).

[26] M. Boström, W. Kunz, and B. W. Ninham, Langmuir **21**, 2619 (2005).

[27] W. Kunz, L. Belloni, O. Bernard, and B. W. Ninham, J. Phys. Chem. B **108**, 2398 (2004).

[28] V. Buch *et al.*, Proc. Nat. Acad. Sci. USA **104**, 7342 (2007).

[29] C. Bai and J. Herzfeld, ACS Cent. Sci. **2**, 225 (2016).

[30] M. D. Baer, I.-F. W. Kuo, D. J. Tobias, and C. J. Mundy, J. Phys. Chem. B **118**, 8364 (2014).

[31] C. J. Mundy, I.-F. W. Kuo, M. E. Tuckerman, H.-S. Lee, and D. J. Tobias, Chem. Phys. Lett. **481**, 2 (2009).

[32] M. K. Petersen, S. S. Iyengar, T. J. F. Day, and G. A. Voth, J. Phys. Chem. B **108**, 14804 (2004).

[33] S. Iuchi, H. Chen, F. Paesani, and G. A. Voth, J. Phys. Chem. B **113**, 4017 (2009).

[34] Y.-L. S. Tse, C. Chen, G. E. Lindberg, R. Kumar, and G. A. Voth, J. Am. Chem. Soc. **137**, 12610 (2015).

[35] T. T. Duignan, D. F. Parsons, and B. W. Ninham, Chem. Phys. Lett. **635**, 1 (2015).

[36] "Supplementary information," (2017).

[37] D. J. Bonthuis, S. I. Mamatkulov, and R. R. Netz, J. Chem. Phys. **144**, 104503 (2016).

[38] H. J. C. Berendsen, J. R. Grigera, and T. P. Straatsma, J. Phys. Chem. **91**, 6269 (1987).

[39] J. E. B. Randles and D. J. Schiffrin, Trans. Faraday Soc. **62**, 2403 (1966).

[40] T. L. Tarbuck, S. T. Ota, and G. L. Richmond, J. Am. Chem. Soc. **128**, 14519 (2006).

[41] A. W. Adamson and A. P. Gast, *Physical Chemistry of Surfaces*, sixth ed. (Wiley, New York, 1997).

[42] Y. Marcus, Chem. Rev. **109**, 1346 (2009).

[43] G. Jones and W. A. Ray, J. Am. Chem. Soc. **63**, 288 (1941).

[44] J. Kessler, H. Elgabarty, T. Spura, K. Karhan, P. Partovi-Azar, A. A. Hassanali, and T. D. Kühne, J. Phys. Chem. B **119**, 10079 (2015).

[45] S. M. Kathmann, I. W. Kuo, C. J. Mundy, and G. K. Schenter, J. Phys. Chem. B **115**, 4369 (2011).

[46] D. J. Bonthuis, S. Gekle, and R. R. Netz, Langmuir **28**, 7679 (2012).

[47] D. J. Bonthuis, D. Horinek, L. Bocquet, and R. R. Netz, Phys. Rev. Lett. **103**, 144503 (2009).